Lattice Parameter of Austenite in Silicon Cast Irons

Jacques Lacaze, Marcos G Lopez, Moukrane Dehmas

ORIGINAL RESEARCH ARTICLE

Lattice Parameter of Austenite in Silicon Cast Irons

JACQUES LACAZE, MARCOS G. LOPEZ, and MOUKRANE DEHMAS

Upon solidification, graphitic cast irons undergo a volume change whose amplitude depends on two opposite terms, the contraction associated with austenite formation and the expansion due to graphite crystallization. During cooling after solidification, further precipitation of graphite occurs that continuously changes the physical properties of the material and possibly affects the eutectoid transformation that transforms the matrix from austenitic to ferritic or ferritic-pearlitic. This work intended to study the density of graphitic cast irons at high temperature, *i.e.*, in the temperature range where the matrix is austenitic. High-temperature laboratory X-rays have been carried out on several alloys containing various carbon and silicon contents to characterize the austenite mean lattice parameter. By complementing these results with literature data, a statistical analysis was carried out that expresses the austenite mean lattice parameter as a function of temperature and composition, evidencing the high uncertainty related to the austenite carbon content. Finally, one of the investigated alloys was submitted to a simultaneous dilatometry and X-ray analysis in a synchrotron from room temperature to 1050 °C. The data are used to discuss the austenite lattice parameter prediction and the possibility of density prediction.

https://doi.org/10.1007/s11661-024-07556-9

I. INTRODUCTION

SILICON cast irons are essentially near-eutectic Fe–C–Si alloys solidifying with precipitation of austenite and graphite. These are alloys easy to cast and highly recyclable, which present a large variety of mechanical properties strongly depending on graphite shape, either lamellar, compacted or spheroidal. As other castable alloys, cast irons can be prone to solidification porosity and shrinkage that can impart casting soundness. However, it is expected that part of the solidification shrinkage of austenite can be compensated by the expansion related to precipitation of graphite,[1,2] even though the details of the volume change at the microstructure level depend on graphite shape (lamellar *vs* spheroidal).[1,3] A previous work attempted to quantify this volume change based on a literature review aimed at expressing the density of liquid and of austenite in the composition range of cast irons, *i.e.*, with quite high contents in carbon and silicon when compared to carbon steels.[4] For austenite, this evaluation was based on the lattice parameter for which the following relation was obtained (Å):

$$a^{\gamma} = 3.57344 + 8.0344{\cdot}10^{-5} \cdot T_C + 0.01865 \cdot w_C + 0.007019 \cdot w_C^2 - 10^{-3} \cdot w_{Si}, \quad [1]$$

where T_C is the temperature expressed in Celsius and w_i is the content in element i of austenite (wt pct). Because of possible precipitation of graphite at high enough carbon content, the austenite composition described with the w_i is not the alloy composition. This is evident for carbon, and w_C will be replaced by w_C^{γ} in the following for stressing this. The content of substitutional elements such as Si, Cu, and Mn, is expected to be slightly higher in austenite when compared to the alloy composition because these elements do not enter in graphite. However, the difference remains low and will have only a small effect on the austenite lattice parameter because the corrections due to alloying elements other than carbon are feeble. Accordingly, the alloy composition in substitutional elements will be used.

Considering the available literature data analyzed in the previous work,[4] it was felt a need for a more extensive work on austenite and this is the purpose of the present report. On a first hand, Appendix A presents a slightly extended literature review with respect to the previous one. It shows high scatter between authors as for the effect of carbon and some indetermination for what concerns silicon. However, Eq. [1] would still appear satisfactory in view of this review and was complemented with the effect of Cu and Mn to read:

JACQUES LACAZE and MOUKRANE DEHMAS are with the CIRIMAT, Université de Toulouse, 31030 Toulouse, France. Contact e-mail: Jacques.lacaze@ensiacet.fr MARCOS G. LOPEZ is with the CIRIMAT, Université de Toulouse and also with the INTEMA, UNMdP – CONICET, B7606BVZ Mar del Plata, Argentina.
Manuscript submitted June 19, 2024; accepted August 9, 2024.

Published online: 05 September 2024

$$a^{\gamma} = 3.57344 + 8.0344{\cdot}10^{-5} \cdot T_C + 0.01865 \cdot w_C^{\gamma} + 0.007019 \cdot \left(w_C^{\gamma}\right)^2 - 10^{-3} \cdot w_{Si} + 1.1{\cdot}10^{-3} \cdot w_{Cu} + 1.1{\cdot}10^{-3} \cdot w_{Mn}. \quad [2]$$

On the other hand, the mean lattice parameter of austenite has been evaluated on a series of alloys with up to 4.1 wt pct carbon and up to 4.3 wt pct silicon during the same experiments than those previously described for the low-temperature domain where these alloys have a fully ferritic matrix.[5] These results are presented in Section II and, unexpectedly, could not be satisfactorily reproduced with Eq. [2]. Together with some selected results on pure Fe, Fe–Si, and Fe–C alloys from the literature review, they were included in a statistical analysis also presented in Section II. Finally, Section III illustrates and discusses the predictions from this analysis. The illustration is based on synchrotron results that gave the continuous evolution of the austenite lattice parameter and change in length upon heating to 1050 °C, holding and then cooling of an alloy with 2.24 wt pct C and 4.26 wt pct Si. This evidences an effect of carbon redistribution that could be converted in an effect on the density changes.

II. EXPERIMENTAL DETAILS AND RESULTS

Table I gives the chemical composition of the alloys that were investigated, namely 9 cast irons and 3 steels as already described.[5] After a heat treatment intended to provide them with a fully ferritic matrix, the samples were subjected to X-rays diffraction analysis in temperature in a Bruker D8 Advance with Cu anode. In this device, heating is provided by a Pt film on which the sample is positioned, and by a radiant furnace which surrounds it. The temperature during the analysis was controlled by a S-type thermocouple located on the Pt film below the sample. An additional S-type thermocouple was welded on the top of the sample, close to where the X-rays beam hits the sample that will be used for the actual sample temperature.

After XRD measurement at room temperature, the furnace temperature was thus successively increased to 100 °C, 300 °C, 500 °C, 700 °C, 850 °C, 1000 °C, and 1150 °C. As soon as the intended temperature was reached, X-rays were recorded in θ to 2θ configuration for 40 minutes. Depending on the run and the sample, only one or two measurements could be made when ferrite was not present, while those where both ferrite and austenite appeared were disregarded because of the risk of induced strain. The collected XRD data were analyzed to extract the mean lattice parameters by Rietveld refinement with the Fullprof software package. These data correspond to the first five characteristic diffraction peaks of austenite, which are {111}, {200}, {220}, {311}, and {222}. However, in some cases, an oxide peak partly superimposed on the first austenite peak; further, the intensity of the fifth peak was most often quite low. It was thus decided to use only the three intermediate peaks for all analyses. Also, the sample temperature changed during the acquisition of some of the XRD patterns, though this relative change was limited to 1 °C to 2 °C in most cases, it reached 10 °C in one case and even 30 °C. The temperature that is reported for each determination was calculated as the weighted average during the acquisition of the three selected peaks. The theoretical error in the lattice parameter determination was considered as three times the standard deviation σ reported by the software. The results are listed in Table II, where also appear two records that were carried out on alloy J upon cooling, using the same procedure as for heating stage. Also, all records on alloy H showed both ferrite and austenite, and no result is reported for this alloy.

Table I. Chemical Composition of the Alloys (Wt Pct)

Alloy	C	Si	Mn	P	S	Cu
A	2.95	1.16	0.35	0.017	0.047	0.81
B	4.03	1.05	0.38	0.033	0.065	0.83
C	2.18	1.19	0.33	0.016	0.056	0.80
D	2.1	1.77	0.36	0.020	0.057	0.81
E	4.13	2.62	0.343	0.021	0.042	0.72
F	2.19	2.55	0.321	0.015	0.059	0.78
G	3.92	1.80	0.419	0.022	0.053	0.80
H	2.97	3.94	0.514	0.022	0.073	0.82
I	2.24	4.26	0.684	0.019	0.113	0.91
J	1.00	0.54	0.011	0.018	0.008	0
K	1.03	1.91	0.017	0.022	0.006	0
L	1.10	3.45	0.024	0.027	0.011	0

In Table II are also listed the carbon contents in austenite at thermodynamic equilibrium calculated with the TCFE8 databank and the software package ThermoCalc.[6] For these calculations, only graphite, ferrite, and austenite phases were taken into account. In the low-temperature range, some experimental records that were expected to show both ferrite and austenite according to the thermodynamic calculations did only show austenite. Accordingly, all calculations were carried out considering only austenite and graphite, not accounting for ferrite and sulfides.

When comparing the results to those predicted with Eq. [2], quite large discrepancies were found. Such discrepancies could be related to many factors, and first of all to uncertainties on the chemical analyses listed in Table I. Standard chemical analyses are expected to give carbon content within ± 0.05 wt pct (combustion technique) and silicon content within ± 0.1 wt pct (sedimentation technique). There are also uncertainties on the actual sample temperature. When analyzing the residues, *i.e.*, the differences between the predicted and measured values, a strong trend was found with the product of silicon and carbon contents of austenite. This triggered a statistical analysis that was performed using the RStudio freeware.[7] The two results on cooling on alloy J were not considered for this statistical analysis and, in order to give enough weight to the 18 selected data listed in Table II, a selection of only 23 literature data was made that contained the results of Basinski

Table II. Results from High-Temperature X-rays Experiments: Sample Temperature, Austenite Lattice Parameter with the Error Provided by Fullprof Software Package, and Austenite Carbon Content w_C^γ Calculated at Thermodynamic Equilibrium with the TCFE8 Databank and the ThermoCalc Software Package

Alloy	T (°C)	a^γ (Å)	Error: ± 3·σ (Å)	w_C^γ(Wt Pct)
A	946	3.7056	0.0024	1.116
B	1011	3.7166	0.0015	1.332
C	868	3.6774	0.0034	0.878
C	1032	3.7118	0.0011	1.200
D	896	3.6732	0.0027	0.878
D	1022	3.6823	0.0042	1.259
E	839	3.6738	0.0015	0.612
E	914	3.6968	0.0023	0.805
F	796	3.6532	0.0009	0.523
F	892	3.6738	0.0020	0.760
G	879	3.6715	0.0024	0.821
G	969	3.7028	0.0046	1.084
I	911	3.6704	0.0008	0.584
J	834	3.6499	0.0017	0.892
J*	957	3.6837	0.0013	0.995
J**	840	3.6668	0.0011	0.910
J**	713	3.6511	0.0007	0.559
K	926	3.6709	0.0016	0.981
L	912	3.6659	0.0006	0.728
L	1010	3.6780	0.0010	0.993

*No graphite according to ThermoCalc calculation; **Upon cooling.

et al. on pure Fe,[8] those of Ridley and Stuart on the Fe–C alloy at 1.02 wt pct C[9] and those of Cockett and Davis for their Fe–Si alloy at 1.45 wt pct Si.[10]

Various attempts were made to account for the square relation with the carbon content shown in Eq. [2] as well as for the product of carbon content and temperature proposed by Chen *et al.*[11] The R^2 correlation coefficient could be increased up to 0.85 but looking at the residues did not show a clear improvement. However, each time the product of the carbon and silicon contents was introduced, it appeared as statistically significant. A last step consisted in limiting the analysis to variables appearing statistically significant, namely temperature, carbon content, and the product of carbon and silicon contents. The following relation would finally express the austenite lattice parameter (Å):

$$a^\gamma = 3.566 + 8.756\cdot10^{-5}\cdot T_C + 2.911\cdot10^{-2}\cdot w_C^\gamma + 3.552\cdot10^{-3}\cdot w_C^\gamma\cdot w_{Si} + 1.1\cdot10^{-3}\cdot w_{Cu} + 1.1\cdot10^{-3}\cdot w_{Mn}. \quad [3]$$

In this equation, the terms in copper and manganese are those from Eq. [2] as they were not evaluated in the present analysis. It is quite interesting that the silicon content alone has no significant effect, in agreement with the poor relationship shown by the only available experimental results by Cockett *et al.*; see Appendix A. It is even more interesting that the known strong thermodynamic interaction between carbon and silicon in austenite seems to effect the austenite lattice parameter through this product term of silicon and carbon contents.

The adjusted R^2 reached a value of 0.72 with residues showing no specific trend. Table III lists the estimated coefficients and the t factors, as well as the probabilities $Pr(|E| > t)$ that show strong statistical significance, where E is the estimated coefficient. To avoid duplicate figures, predictions made with Eq. [3] are compared to those made with Eq. [2] in Figures 6, 8, and 9 of the Appendix A. It is seen that the present analysis is as satisfactory as was the previous one for the literature data and, as mentioned above, much better than the previous one for the experimental results of this study.

Even though the statistics of the analysis are satisfactory, some differences between predictions and measurements still appear as seen in Figure 1. In this figure, the dots are data from the literature, while the circled dots relate to the present results and are seen to be those with the largest scatter. The few results showing the largest differences have been identified in Figure 1. Using Eq. [3], an error of 10 °C on the sample temperature would lead to an error of less than $1\cdot10^{-3}$ Å that is one order of magnitude lower than some of the differences between predicted and experimental values. Another possible source of error is the carbon content in austenite, that should differ by 0.2 to 0.3 wt pct to change the lattice parameter by 0.01 Å as needed. A first explanation could be a poor description of the carbon content in austenite in the TCFE8 database, the accuracy of which is unfortunately difficult to assess. A more likely reason is that the samples did not reach complete equilibrium after the 40 minutes of temperature holding, particularly if the spatial distribution of graphite precipitates is coarse.

III. DISCUSSION

The final aim of this work being to predict the density of austenite in silicon cast irons during cooling after casting, it is of definite interest to consider the results of an experiment carried out on alloy I using high-energy X-ray diffraction (HEXRD) at the P07 beamline of the PETRA III in DESY (Deutsches Elektronen-Synchrotron, Hamburg, Germany). The fully ferritized sample was inductively heated to 1050 °C at 20 °C/min with a S-type thermocouple welded close to the analyzed volume. The sample was then held at that temperature for 30 minutes and finally cooled to room temperature at the same rate of 20 °C/min. A 2D-dectector PerkinElmer XRD 1621 Flat Panel with a resolution of 2048 by 2048 pixels placed at 1513 mm in transmission was employed in order to collect the Debye–Scherrer rings for diffraction angle 2θ between 0 and 10.8 deg, and with an acquisition time of 5 seconds. The Debye–Scherrer rings were circularly integrated with Fit2D software to obtain standard 1D diffractogram (I vs 2θ). The error in the lattice parameter due to the detector resolution, in addition to the error inherent in the refinement method, was estimated ± 1.10^{-3} Å.

Table III. Statistical Analysis Corresponding to the First Four Coefficients of Eq. [3]

Parameter	Estimate, E	Standard Error	t Value	$Pr(\|E\|>t)$
Constant	3.566	$1.3 \cdot 10^{-2}$	278	$< 2 \cdot 10^{-16}$
Temperature	$8.756 \cdot 10^{-5}$	$1.1 \cdot 10^{-5}$	7.7	$3.5 \cdot 10^{-9}$
w_C^γ	$2.911 \cdot 10^{-2}$	$3.7 \cdot 10^{-3}$	7.9	$1.9 \cdot 10^{-9}$
$w_C^\gamma \cdot w_{Si}$	$3.552 \cdot 10^{-3}$	$1.7 \cdot 10^{-3}$	2.1	0.044

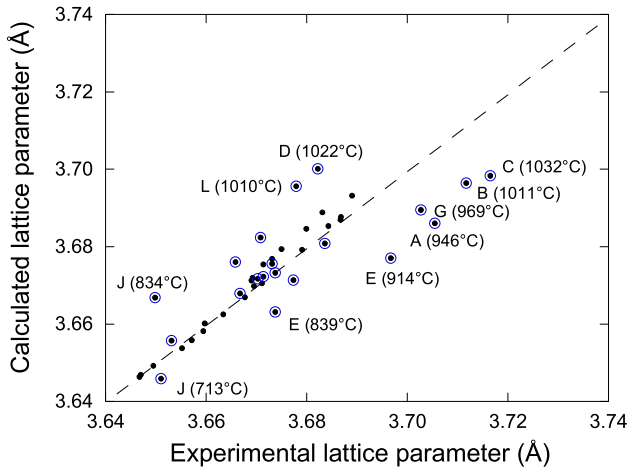

Fig. 1—Comparison of predicted to measured lattice parameter of austenite. Dots are data from literature (see text), while circled dots are results from the present study. The dashed line is the bisector and the samples with largest discrepancies have been identified with the holding temperature indicated within brackets.

Austenite appeared at about 860 °C and the matrix became fully austenitic at 912 °C that was used as a reference for plotting the change in the relative austenite lattice parameter $\Delta a^\gamma/a^\gamma$ shown in Figure 2(a). As the temperature further raised up to 1050 °C, the lattice parameter increased steeply. During the holding at 1050 °C, the lattice parameter continued to increase, though at a slower pace, and then stabilized in about 15 minutes. This delay appears to be the time needed for austenite to become saturated in carbon by partial dissolution of the graphite precipitates. Using the provisional value of the diffusion coefficient of carbon assessed by Ågren[12] for pure Fe, $D_C^\gamma = 2.343 \cdot 10^{-5} \cdot \exp\left(-\frac{17767}{T_K}\right)$ ($m^2\ s^{-1}$), where T_K is the temperature in Kelvin, one can calculate the segregation index δ defined by Flemings and collaborators as $\delta = \exp\left(-\pi^2 \cdot D_C^\gamma \cdot t/L^2\right)$,[13] where t is the homogenization time and L the diffusion length. For a holding time t = 900 seconds at 1050 °C, the diffusion length over which δ decreases to 1 pct of its initial value is higher than 250 μm, far larger than half the maximum distance between graphite precipitates in alloy I as seen with the micrograph in Figure 2(b). This sustains a complete homogenization of carbon during this length of time for this alloy, though this conclusion might not be valid for other alloys with coarser graphite spatial distribution at lower temperature as discussed above.

The actual evolution of the austenite lattice parameter during the experiment is shown in Figure 3(a), where the arrows indicate heating and cooling ramps. The bump appearing at the beginning of the cooling part is due to a small instability of the furnace that cannot be noticed in Figure 2(a) because of the used scale. The temperature derivative of the curve in Figure 3(a) is plotted in Figure 3(b), after removing the part corresponding to the holding and having applied a mobile average of 25 measurements. If the bump is not considered, it is noticeable that the experimental slope is the same upon heating and cooling between 950 °C and 1050 °C, which would mean that the transfer of carbon atoms from graphite to austenite upon heating and from austenite to graphite upon cooling proceeds at the same rate in this temperature range. However, the slopes are different below 950 °C and this is not before reaching 850 °C that the slope started to decrease upon cooling, suggesting a significant slowing down of the rate of transfer of carbon to graphite below 950 °C.

The evolution of the carbon content in austenite at thermodynamic equilibrium between 800 °C and 1050 °C was calculated using TCFE8 and the Thermo-Calc software package. These values were then introduced in Eq. [3] and the results are also reported in Figure 3(a). The upper value at 1050 °C is in quite good agreement with the experimental stabilized value, though slightly larger, while the predicted slope on cooling appears steeper than the experimental one as expected from the above discussion. This leads to the fact that austenite certainly remains somewhat supersaturated in carbon upon cooling at 20 °C/min. This has been previously noticed for spheroidal graphite cast irons investigated with dilatometry under quite similar conditions[14] and may have consequences on the eutectoid transformation.[15]

Figure 4 shows the evolution of the lattice parameter of the matrix from room temperature to 1050 °C, that is for both ferrite for temperature up to more than 800 °C and for austenite for temperature above 860 °C upon heating and down to 700 °C upon cooling. The dashed lines are calculated using Eq. [4] in the previous work for ferrite[5] and Eq. [3] from the present work for austenite. There is a slight overestimation for ferrite for both heating and cooling, and it is clearly seen that the measured lattice parameter is affected by the phase change in the upper temperature range. On the other hand, the slight shift between the records upon heating and cooling in the ferrite domain is within the expected accuracy of the measurements. For austenite, the measured lattice parameter is far below the predicted

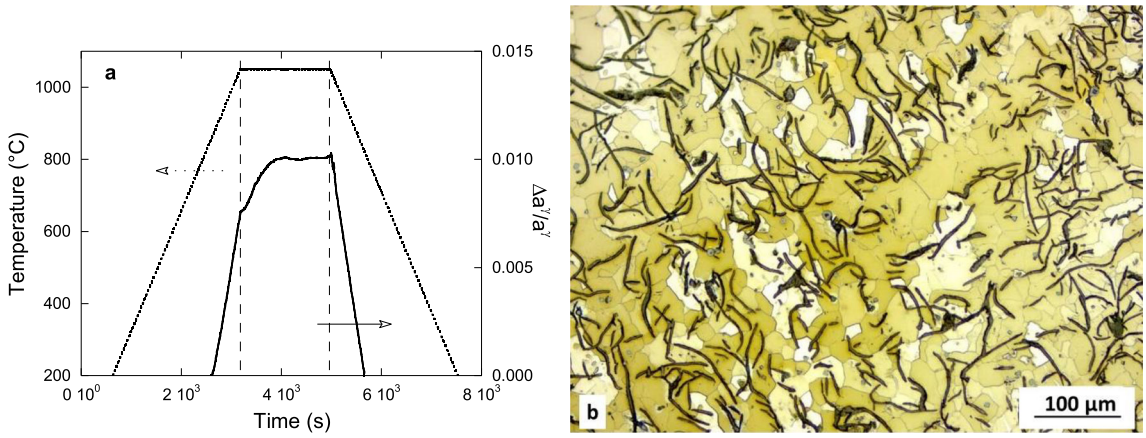

Fig. 2—(*a*) Evolution with time of the sample temperature and of the relative austenite lattice parameter during the HEXRD experiment. (*b*) Optical micrograph of the sample.

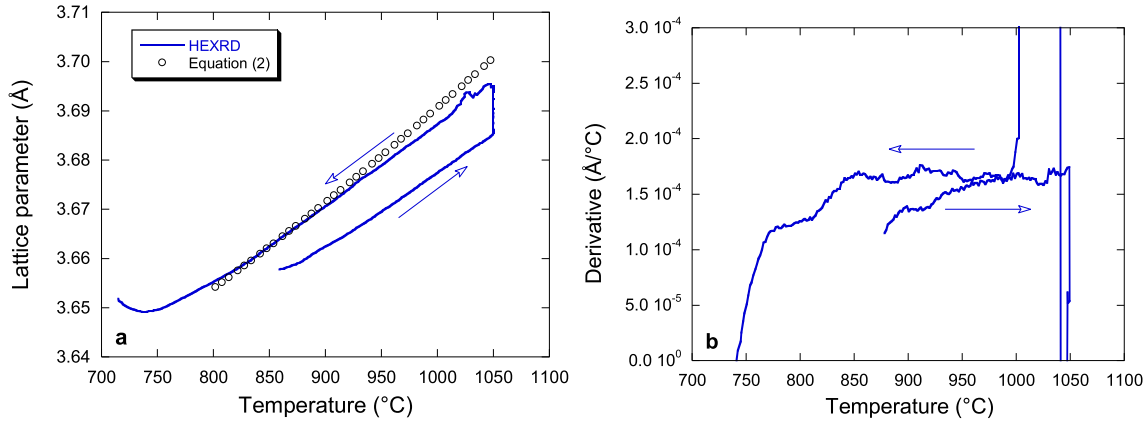

Fig. 3—(*a*) Experimental evolution with temperature of the austenite lattice parameter upon heating, holding at 1050 °C, and cooling (solid line) and predicted evolution between 900 °C and 1050 °C (circles). (*b*) Temperature derivative of the curve in (a) after removing the part corresponding to the holding and applying a moving average (25 successive measurements).

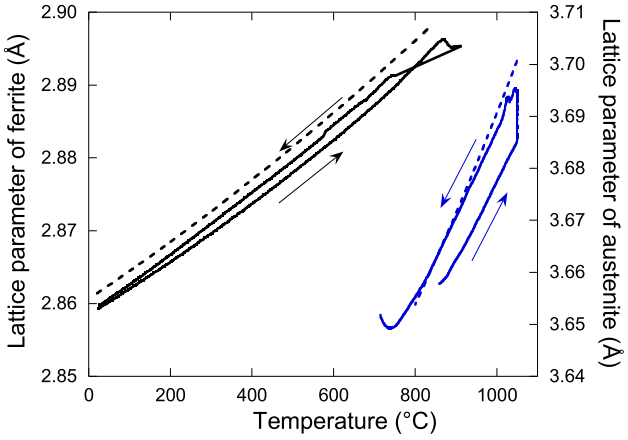

Fig. 4—Solid lines show experimental evolution of the lattice parameter of ferrite (left scale) and of austenite (scale to the right) as function of temperature. Dashed lines are calculated; see text.

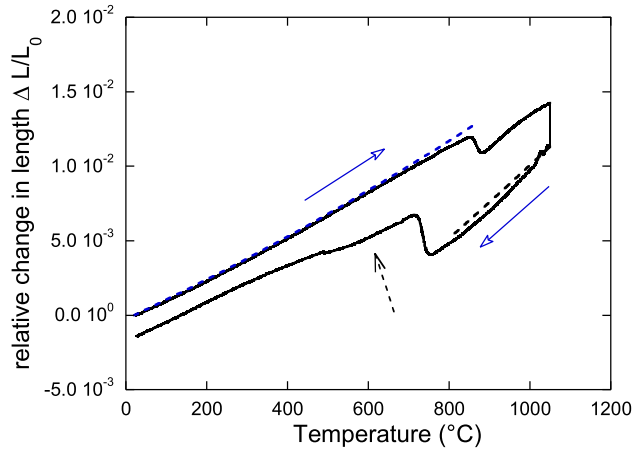

Fig. 5—Relative change in length of alloy I upon cycling from room temperature to 1050 °C. The dashed lines are calculated; see text.

one upon heating as discussed above, while the prediction appears quite satisfactory upon cooling with the temperature scale used in Figure 4.

Finally, Figure 5 presents with solid lines the relative change in length of the sample, $\Delta L/L_0$, during the temperature cycle, where L_0 is its length at room

temperature. The contraction on temperature rise associated with the transition from ferrite to austenite and the expansion on cooling associated with the reverse transformation are easily identifiable. They are located around 100 °C apart and take place within a temperature range of 30 °C to 40 °C. On cooling, the curve shows a positive curvature from 720 °C to 490 °C, as indicated by the dashed arrow, and then runs parallel to the curve on heating at lower temperatures. This unexpected behavior must be associated with graphite precipitation as the matrix is progressively cleared of carbon supersaturation.

For isotropic materials, the relative change in length recorded by dilatometry is related to the change in density by the following relation[16]:

$$\frac{\Delta L}{L_0} = \left(\frac{\rho(T_0)}{\rho(T)}\right)^{1/3} - 1, \qquad [4]$$

where $\rho(T_0)$ and L_0 are the density and sample length at a reference temperature T_0 and $\rho(T)$ that at T.

The calculation of the density of the cast iron with a ferritic or an austenitic matrix is described in Appendix B, where some recent literature data are also considered. From this, the change in length from room temperature to 860 °C was calculated using Eq. [4] for a ferritic matrix with the reference temperature set at room temperature, and also for an austenitic matrix from 1050 °C to 800 °C with 1050 °C as reference temperature. These calculations appear as dashed lines in Figure 5. For heating from room temperature to the end of the ferritic domain, an excellent agreement is seen except at the highest temperatures. An attempt has been made to account for the effect of carbon dissolved in ferrite and this effectively decreased the difference but did not explain all of it. For austenite upon cooling from 1050 °C, the prediction can be seen as satisfactory though the agreement is not as good as for the low-temperature range with ferrite. In summary, it can be stated that the present approach would certainly allow predicting relative change of length when the material keeps to the ferritic domain, as well as the change of length in the austenitic domain upon cooling after solidification.

IV. CONCLUSION

An expression for the determination of the austenite lattice parameter in cast iron could be obtained, on the basis of considering both the experimental values from this investigation as well as some other significant results from literature. The statistical analysis from this work reveals that, besides of the clear effect of temperature and carbon content, the product of carbon and silicon contents has a significant effect on the lattice parameter. Even though the statistics of the analysis are satisfactory, some differences between predictions and measurements are observed that are probably due to uncertainties in the carbon content of austenite. By relating the lattice parameter to density, relative change in length recorded by dilatometry can be predicted leading to the conclusion that the evolution of density upon cooling from high temperature in the austenitic range as well as upon heating from room temperature in the ferritic range are conveniently described.

ACKNOWLEDGMENTS

Thanks are due to A. Dioszegi, B. Domeij, and L.-V. Diaconu for providing the alloys for this work. The authors also acknowledge people at the accelerator DESY (Hamburg, Germany), a member of the Helmholtz Association HGF, for the provision of experimental facilities. Parts of this research were carried out at PETRA III and we would like to thank Dr. E. Maawad for assistance in using the P07 beamline. Beam time was allocated for proposal I-20230170 EC.

FUNDING

Open access funding provided by Institut National Polytechnique de Toulouse.

CONFLICT OF INTEREST

The authors declare that they have no conflict of interest.

APPENDIX A: LATTICE PARAMETER OF AUSTENITE IN SILICON CAST IRONS

In a previous work,[4] results on pure Fe by Basinski *et al.*[8] and of Ridley and Stuart on Fe–C alloys[17] gave the following relation between the lattice parameter of austenite, a^{γ} (Å), the temperature expressed in Celsius, T_C, and the carbon content in wt pct, $w_{C,}$:

$$a^{\gamma} = 3.57344 + 8.0344 \cdot 10^{-5} \cdot T_C + 0.01865 \cdot w_C + 0.007019 \cdot w_C^2. \qquad [5]$$

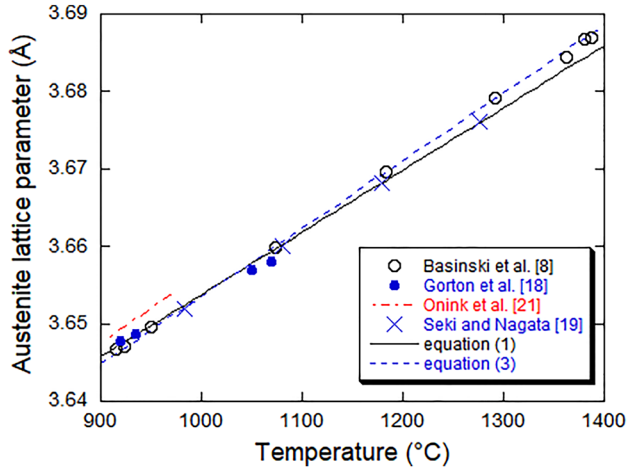

Fig. 6—Lattice parameter of pure Fe in the austenite field.

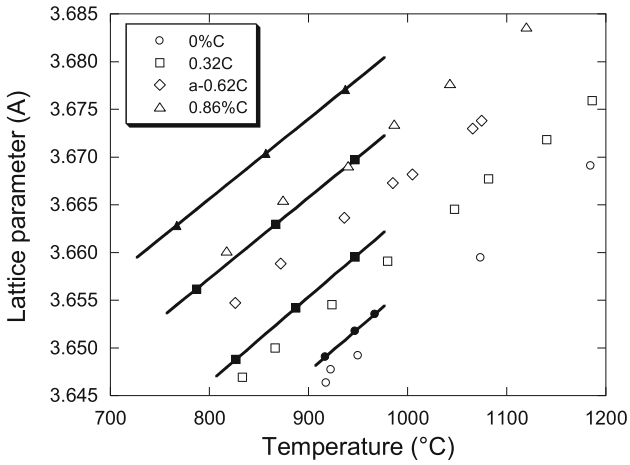

Fig. 7—Comparison of the results of Onink *et al.*[21] in solid lines (0, 0.3, 0.6, and 0.8 wt pct C) with the results of Ridley and Stuart[17] for similar carbon contents represented with the same symbols, solid for Onink *et al.* and open for Ridley and Stuart.

This work put some strong weight on the extensive study of Ridley and Stuart[17] who investigated Fe–C alloys with up to 1.44 wt pct C for temperature between 800 °C and 1200 °C. Though the fit obtained was excellent, it might appear reasonable to compare the predictions made with this relation to other available data that were previously not considered.

At first, Figure 6 shows data for the austenite field of pure iron, including high-temperature measurements of Gorton *et al.*[18] and Seki and Nagata[19] in addition to those of Basinski *et al.*[8] These results are in excellent agreement between each other. Note that Basinski *et al.* gave their results in *kX* as the correction factor was uncertain at that time. Ridley and Stuart[17] used these results after correction with the factor of 1.00202 determined by Bragg and Armstrong-Wood[20] and the same has been done here.

The solid line in Figure 6 corresponds to the two first terms of Eq. [5] and it is seen it reproduces quite well all data but a few values from Basinski *et al.* at the highest

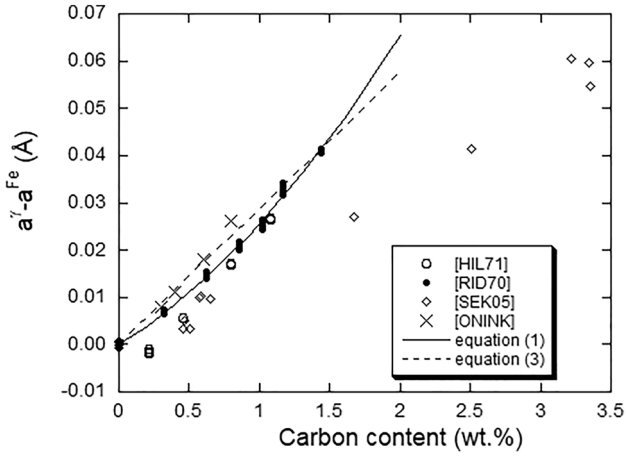

Fig. 8—Difference between the austenite Fe–C parameter and that of pure Fe at the same temperature.

temperatures. The equation given by Onink *et al.*[21] for the temperature range [1180, 1250] (K) has also been plotted and locates 0.0025 Å above other results. Finally, the dashed line represents Eq. [3] in the main text and fits better the results of Basinski *et al.*, which is expected as these were the values selected for the statistical analysis.

In addition to the work by Ridley and Stuart on Fe–C alloys, other works reporting data on the effect of carbon on the austenite lattice parameter are by Onink *et al.*,[21] Seki and Nagata[19], and a few results by Hillert *et al.*[22] Onink *et al.*[21] investigated alloys with up to 0.8 wt pct C for a maximum temperature range between 730 °C and 980 °C. These authors did not give much experimental detail but provided a linear regression function of temperature for each of their five samples. In Figure 7, their results for 0, 0.3, 0.6 and 0.8 wt pct C are compared to those of Ridley and Stuart for similar carbon contents (indicated in the insert). Onink's results are systematically above those of Ridley and Stuart as was already noted for pure Fe-γ, but it is here seen that the variance increases significantly with the carbon content.

For focusing on the effect of carbon, the difference between the measured a^{γ} value and that for pure Fe, a^{Fe}, at the same temperature was evaluated as shown in Figure 8, where the solid curve is the evolution calculated with the last two terms of Eq. [5]. As expected, the whole set of results from Ridley and Stuart (more than 40 measurements) lie on this curve. Results by Onink *et al.*[21] were calculated using the equations provided by the authors for the maximum temperature of 977 °C (1250 K) of the investigated interval, namely by calculating the difference to the value given for pure Fe by the authors. The choice of this particular temperature was made as it corresponds to the maximum difference between data by Onink *et al.* and those by Ridley and Stuart in Figure 7. As stated above, it is thus evidenced that the discrepancy increases with the carbon content, though the reported values are not so far from those predicted by Eq. [5].

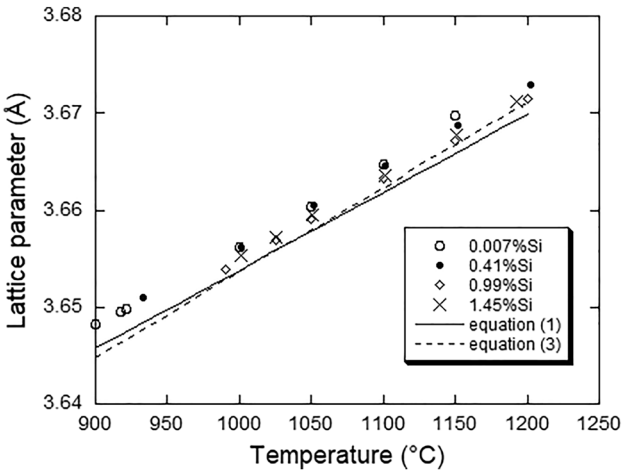

Fig. 9—Experimental values of austenite lattice parameter for Fe–Si alloys from Cockett and Davis[10] and linear relation according to Eq. [1] (solid line) and to Eq. [3] (dashed line) for pure Fe.

Hillert *et al.*[22] reported a few results obtained during a study on cementite dissolution in Fe–Cr–C alloys at temperature from 770 °C to 910 °C. They gave very little details on their experiments so that a low weight should be put on their results that are reported in Figure 8 using Eq. [5] to evaluate the lattice parameter of pure Fe. Their values are quite close to predictions at carbon contents higher than 0.5 wt pct but would badly extrapolate at zero carbon content. Finally, Seki and Nagata[19] reported a few high-temperature data corresponding to austenite both undersaturated and supersaturated in carbon. When reported on Figure 8 using again Eq. [5] for pure Fe, their values are quite close to predictions for undersaturated alloys (less than 1 wt pct C), while they strongly deviate for oversaturated ones. Because it is not expected that carbon supersaturation in cast iron austenite could achieve the high values reported by Seki and Nagata, it could be concluded that Eq. [5] would give an appropriate estimate of the effect of carbon on the lattice parameter of austenite. In turn, the linear carbon effect indicated by Eq. [3] of the main text predicts an effect closer to that proposed by Onink *et al.*, but still in general good agreement with Eq. [1].

Owing to the shape of the gamma loop in the Fe–Si phase diagram, the effect of silicon on the lattice parameter of Fe-γ in the Fe–Si system can be studied only for silicon contents lower than about 2 wt pct. For steels, the most usual way consisted to include silicon in statistical studies as was done in the reference work by Dyson and Holmes.[23] In this work, silicon was seen to slightly decrease the lattice parameter of 16/25 Cr–Ni steels but to slightly increase it for 18/10 Cr–Ni steels. Accordingly, it did not appear in the final regression analysis reported by these authors, while Irvine *et al.*[24] reported a contraction of 0.0005 Å/at. pct for stainless steels that was selected by Chen *et al.*[11] for cast irons. Studying Fe–Si alloys, Cockett and Davis[10] also reported a contraction of the austenite lattice of 0.0003 Å/wt pct Si on the basis of their results at 1050 °C. However, plotting the whole set of their results as done in Figure 9 shows high scattering of the silicon effect. This suggests it could be wise to consider that there is no significant effect of silicon on its own, and this was accepted in Eq. [3] of the main text. The lines corresponding to pure Fe according to Eqs. [1] and [3] are located below all the results of Cockett and Davies, in particular those results obtained on the nearly pure Fe alloy at 0.007 wt pct Si.

Li *et al.*[25] have investigated the room temperature effect of Mn on ferrite and austenite in Fe–Mn alloys. At high enough Mn content, the alloy is austenitic and the lattice parameter increases by 0.0011 Å/pct Mn, either in atom or weight owing to the similarity of the molar mass of Fe and Mn. Velthuis *et al.*[26] measured the effect of Cu on the lattice parameter of austenite for two Fe–Cu alloys, in the temperature range of 1160 K to 1350 K. Using the proposed equation for each alloy, an average increase of the austenite lattice parameter of $1.08{\cdot}10^{-3}$ Å between the alloy at 0.8 at. pct Cu and that at 1.7 at. pct Cu is obtained. This converts to an increase of $1.1{\cdot}10^{-3}$ Å/wt pct Cu that appears much larger than the $0.4{\cdot}10^{-3}$ Å/at. pct Cu suggested by the authors. With all the data reported above, the lattice parameter of austenite is expressed with the following equation:

$$a^{\gamma} = 3.57344 + 8.0344{\cdot}10^{-5}\cdot T_C + 0.01865\cdot w_C + 0.007019\cdot w_C^2 - 10^{-3}\cdot w_{Si} + 1.1{\cdot}10^{-3}\cdot w_{Cu} + 1.1{\cdot}10^{-3}\cdot w_{Mn}. \quad [6]$$

APPENDIX B: DENSITY OF CAST IRONS

Cast irons are considered here as two-phase materials consisting of graphite precipitates within a matrix φ that is either ferritic or austenitic. The inverse of the density ρ of the composite is its specific volume v that is given as follows[16]:

$$v = \frac{1}{\rho} = \frac{f^{gra}}{\rho^{gra}} + \frac{f^{\varphi}}{\rho^{\varphi}}, \quad [7]$$

where f^{gra} and f^{φ} are the mass fraction of graphite and matrix, and ρ^{gra} and ρ^{φ} their density. For theoretical density calculation (no porosity), the sum of these mass fractions is 1:

$$f^{gra} + f^{\varphi} = 1. \quad [8]$$

The mass fraction of graphite is obtained by the following mass balance:

$$f^{gra} = \frac{w_C^0 - w_C^{\varphi}(T_C)}{w_C^{gra} - w_C^{\varphi}(T_C)}, \quad [9]$$

where w_C^0 is the carbon content of the alloy, $w_C^{\varphi}(T_C)$ is the carbon content of the matrix φ at the considered temperature T_C, and w_C^{gra} is the carbon content in graphite (all w in wt pct). For the calculations carried

Table IV. Carbon and Silicon Contents (wt pct) (also 0.34 to 0.41 wt pct Mn), Experimental Values of Solidus Temperature (°C), and of Density (kg m^{-3}) of the Alloys Investigated by Hellström *et al.*,[28] and Density Values Calculated in the Present Work

Alloy Reference	Carbon	Silicon	Solidus Temperature	Experimental Density	Calculated Density
C050	0.59	1.75	1356	7213	7194
C080	0.97	2.01	1305	7184	7144
C100	1.08	1.88	1266	7177	7162
C125	1.14	1.89	1243	7200	7164
C150	1.49	2.02	1222	7055	7113

out in this work, the equilibrium values of $w_C^{\gamma}(T_C)$ have been used, meaning that Eq. [9] turns out to be the lever rule. For ferrite, the calculations shown in Figure 4 were performed with $w_C^{\alpha}(T_C)$ set to zero.

The following expression of the graphite density will be used (g cm^3)[27]:

$$(\rho^{gra})^{-1} = 0.4419 + 10.5 \cdot 10^{-6} \cdot T_C. \quad [10]$$

The density of the matrix can be calculated from the lattice parameter as follows[16]:

$$\rho^{\varphi} = \frac{n^{\varphi} \cdot M_m^{\varphi}}{\left(1 - x_C^{\varphi}\right) \cdot (a^{\varphi})^3 \cdot N_A} \quad [11]$$

in which n^{φ} is the number of substitutional sites per unit cell (2 for bcc ferrite and 4 for fcc austenite) and a^{φ} its lattice parameter, M_m^{φ} is the molar mass of the matrix, x_C^{φ} is the atom fraction of carbon, and N_A is the Avogadro number. Inserting Eq. [11] in Eq. [7] leads to the following expression for the cast iron density:

$$\rho = \left[f^{gra} \cdot (\rho^{gra})^{-1} + (1 - f^{gra}) \cdot \frac{\left(1 - x_C^{\varphi}\right) \cdot (a^{\varphi})^3 \cdot N_A}{n^{\varphi} \cdot M_m^{\varphi}} \right]^{-1} \quad [12]$$

Very little data are available in the literature to verify the validity of the expression of a^{γ}, which determines the quality of the density evaluation. The evaluation of the density of single-phase austenite at the solidus temperature of a few Fe–C–Si alloys has been reported by Hellström *et al.*[28] Table IV lists the composition of the alloys for which the authors reported density values that were picked up from their Figure 4 together with the relevant temperature. With the composition and the temperature, the austenite lattice parameter was calculated using Eq. [3] in the text and the density with Eq. [11]. It is seen in Table IV that the calculated values are in quite good agreement with the experimental ones, and it is noticeable that the increase in solidus temperature because of carbon decrease compensates each other so that the density shows little change.

REFERENCES

1. M. Hillert: in *Recent Research on Cast Iron*, H.D. Merchant, ed., 1968, pp. 101–27.
2. M. Hillert: *Phys. Metall. Cast Iron, E-MRS Proc.*, 1985, vol. 34, pp. 233–37.
3. J.M. Théret and G. Lesoult: *Hommes et Fonderie*, 1984, pp. 19–30.
4. J. Lacaze, J. Sertucha, and U. de la Torre: *Int. J. Metalcast.*, 2023, vol. 17, pp. 1493–1506.
5. M. Lopez, M. Dehmas, and J. Lacaze: *Metall. Mater. Trans.*, 2024, vol. 55, pp. 1908–15.
6. Thermo-Calc Software TCFE version 8, https://thermocalc.com/products/databases/. Accessed 1 Oct 2023.
7. Posit, RStudio 2023.06.2 Build 641, https://posit.co/. Accessed 1 Oct 2023.
8. Z.S. Basinski, W. Hume-Rothery, and A.L. Sutton: *Proc. R. Soc. Lond. Ser. A Math. Phys. Sci.*, 1955, vol. 229, pp. 459–67.
9. N. Ridley and H. Stuart: *Met. Sci. J.*, 1970, vol. 4, pp. 219–22.
10. G.H. Cockett and C.D. Davis: *J. Iron Steel Inst.*, 1963, vol. 201, pp. 110–15.
11. Q. Chen, E.W. Langer, and O.N. Hansen: *Scand. J. Metall.*, 1994, vol. 23, pp. 3–8.
12. J. Ågren: *Acta Metall.*, 1989, vol. 37, pp. 181–89.
13. M.C. Flemings: *Solidification Processing*, McGraw-Hill Inc, New York, 1974.
14. F. Hellal, J. Lacaze, and A. Hazotte: *Mater. Sci. Technol.*, 1999, vol. 15, pp. 773–78.
15. J. Lacaze and V. Gerval: *ISIJ Int.*, 1998, vol. 38, pp. 714–22.
16. A. Jablonka, K. Harste, and K. Schwerdtfeger: *Steel Res.*, 1991, vol. 62, pp. 24–33.
17. N. Ridley and H. Stuart: *Br. J. Appl. Phys.*, 1968, vol. 1, pp. 1291–95.
18. A.T. Gorton, G. Bitsianes, and T.L. Joseph: *Trans. Metall. Trans. AIME*, 1965, vol. 233, pp. 1519–25.
19. I. Seki and K. Nagata: *ISIJ Int.*, 2005, vol. 45, pp. 1789–94.
20. W. Bragg and E. Armstrong-Wood: *J. Am. Chem. Soc.*, 1947, vol. 69, p. 2919.
21. M. Onink, C.M. Brakman, F.D. Tichelard, et al.: *Scripta Metall. Mater.*, 1993, vol. 29, pp. 1011–16.
22. M. Hillert, K. Nilsson, and L.E. Törndahl: *J. Iron Steel Inst.*, 1971, vol. 209, pp. 49–66.
23. D.J. Dyson and B. Holmes: *J. Iron Steel Inst.*, 1970, vol. 208, pp. 489–74.
24. K.J. Irvine, D.T. Llewellyn, and F.B. Pickering: *J. Iron Steel Inst.*, 1961, vol. 199, pp. 153–75.
25. C. Li, F. Sommer, and E.J. Mittemeijer: *Mater. Sci. Eng. A*, 2002, vol. 325, pp. 307–19.
26. S.G.E. Te Velthuis, J.H. Root, J. Sietsma, HTh. Rekveldt, and S. Van Der Zwaag: *Acta Mater.*, 1998, vol. 46, pp. 5223–28.
27. P. Dietrich and G. Lesoult: in: *State of the art computer simulation of casting and solidification processes*, Les éditions de Physique, H. Fredriksson, ed., 1986, pp. 225–35.
28. K. Hellström, V.L. Diaconu, and A. Dioszegi: *China Foundry*, 2020, vol. 17, pp. 127–36.